

See discussions, stats, and author profiles for this publication at: <https://www.researchgate.net/publication/276250102>

# Transport of Polarons in Graphene Nanoribbons

ARTICLE *in* JOURNAL OF PHYSICAL CHEMISTRY LETTERS · JANUARY 2015

Impact Factor: 7.46 · DOI: 10.1021/jz502460g

---

CITATION

1

READS

19

## 5 AUTHORS, INCLUDING:



Wiliam Ferreira da Cunha

University of Brasília

44 PUBLICATIONS 174 CITATIONS

[SEE PROFILE](#)



Antonio Luciano A. Fonseca

University of Brasília

80 PUBLICATIONS 530 CITATIONS

[SEE PROFILE](#)



Geraldo Magela e Silva

University of Brasília

90 PUBLICATIONS 509 CITATIONS

[SEE PROFILE](#)



Sven Stafström

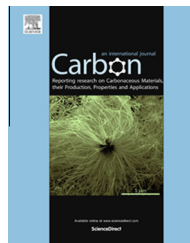
Linköping University

224 PUBLICATIONS 5,311 CITATIONS

[SEE PROFILE](#)



ELSEVIER

Available at [www.sciencedirect.com](http://www.sciencedirect.com)**ScienceDirect**journal homepage: [www.elsevier.com/locate/carbon](http://www.elsevier.com/locate/carbon)

# Impurity effects on polaron dynamics in graphene nanoribbons

Wiliam Ferreira da Cunha <sup>a</sup>, Luiz Antonio Ribeiro Junior <sup>b,a,\*</sup>,  
Antonio Luciano de Almeida Fonseca <sup>a</sup>, Ricardo Gargano <sup>a,c,d</sup>, Geraldo Magela e Silva <sup>a</sup>

<sup>a</sup> Institute of Physics, University of Brasilia, 70.919-970 Brasilia, Brazil

<sup>b</sup> Department of Physics, Chemistry and Biology (IFM), Linköping University, SE-581 83 Linköping, Sweden

<sup>c</sup> Department of Chemistry, University of Florida, Quantum Theory Project, Gainesville, FL 32611, USA

<sup>d</sup> Department of Physics, University of Florida, Quantum Theory Project, Gainesville, FL 32611, USA

## ARTICLE INFO

### Article history:

Received 25 February 2015

Accepted 23 April 2015

Available online 30 April 2015

## ABSTRACT

The impurity effects on the dynamics of polarons in armchair graphene nanoribbons are numerically investigated in the scope of a two-dimensional tight-binding approach with lattice relaxation. The results show that the presence of an impurity changes significantly the net charge distribution associated to the polaron structure. Moreover, the interplay between external electric field and the local impurities plays the role of drastically modifying the polaron dynamics. Interestingly, nanoribbons containing mobile polarons are noted to take place even when considering high impurity levels, which is associated with the highly conductive character of the graphene nanoribbons. This investigation may enlighten the understanding of the charge transport mechanism in carbon-based nanomaterials.

© 2015 Elsevier Ltd. All rights reserved.

## 1. Introduction

Carbon-based nanomaterials [1–3] are pointed as promising solutions to the development of a novel electronic device technology that presents smaller environmental impact when compared to its inorganic counterparts [4]. Due to unique traits such as high mechanical strength, easy of synthesis, strict two-dimensionality, and low cost, graphene has attracted huge interest to the design of photovoltaic [5], energy storage [6], and field-effect transistor applications [7]. Significant efforts have been performed theoretically [8–10] and experimentally [11,12] in order to understand the role played by dopants on the charge transport mechanism in graphene films and nanoribbons. Importantly, these works have investigated impurity effects on the charge transport from the framework of metallic-like behavior. Nonetheless, theoretical

studies considering the semiconducting-like physical picture for charge transport mechanism under influence of impurities are still insufficient. It is well established that armchair graphene nanoribbons (GNR) present finite bandgaps in the range of semiconducting materials. This feature makes GNR of special interest for the carbon-based electronics community. Therefore investigations on impurity effects, particularly on GNRs, are extremely required.

Very recently, the charge transport properties of a GNR in the presence of impurities was experimentally studied using an ultra high vacuum environment [13]. The findings have shown that the field-effect mobility of charge in graphene was observed to be  $360 \text{ cm}^2/(\text{V}\cdot\text{s})$  for holes and  $410 \text{ cm}^2/(\text{V}\cdot\text{s})$  for electrons prior from doping. Moreover, when the doping with certain levels of Cesium was considered, the field-effect mobility is considerably decreased for values which lie,

\* Corresponding author at: Department of Physics, Chemistry and Biology (IFM), Linköping University, SE-581 83 Linköping, Sweden.  
E-mail address: [luiju@ifm.liu.se](mailto:luiju@ifm.liu.se) (L.A. Ribeiro).

approximately, in the range of  $20\text{--}120 \text{ cm}^2/(\text{V}\cdot\text{s})$  for both electrons and holes. In a theoretical work, Lherbier and colleagues reported the charge transport in boron (and nitrogen) doped 2D graphene sheets using the Kubo-Greenwood approach, which allows to evaluate the resulting charge mobilities of a system with impurity concentrations ranging within 0.5–4.0% [14]. Their results showed that, for doping concentrations around 4.0%, the conduction may be influenced by quantum interference effects. As a result of the doping process, the electron and hole mobilities and conductivities are shown to be asymmetric regarding the Dirac point, with minimal conductivities ranging between 2 and  $8 \text{ e}^2/\text{h}$  depending mainly on the doping level and the carrier density. Recently it was reported an *ab initio* study of the effect of both *p*-type (*n*-type) impurities on charge transport in GNRs, in which the doping was achieved by boron (nitrogen) atom substitution within the carbon matrix [15]. Remarkably, it was found that the chemical doping could be used to enlarge the band gap of a fixed GNR width, which may result in the improvement of the device performance. Some relevant theoretical studies have also reported the influence of other kind of atomic doping strategies using Oxygen, Phosphorus, Sulfur, and Silicon [16,17]. The results obtained by Chen and coworkers [16] show that, combining the Boltzmann transport equation with the deformation potential theory, large charge carrier mobilities are maintained upon noncovalent functionalization of graphene. On the other hand, there are strong evidences that the presence of impurities in the lattice are malignant to the charge transport efficiency in organic semiconductors. Thereby, investigations about charge transport mechanism in the semiconducting regime for GNRs, when impurity effects are taken into account, albeit yet not performed, are believed to be of fundamental importance.

In this paper, an extensive numerical investigation of impurity effects on the charge transport mechanism in GNRs is performed in the framework of a nonadiabatic evolution method. The interaction between the net charge associated to a polaron structure and the impurities is investigated in systems subjected to different electric field strengths. Molecular dynamics is performed using a two-dimensional tight-binding approach which includes lattice relaxation. The aim of this work is to give a physical picture of the charge transport mechanism in GNRs, mainly when impurity effects are taken into account, and contribute to the understanding of these important processes. This investigation may enlighten the understanding of the charge transport mechanism in the next-generation of carbon-based nanomaterials.

## 2. Methodology

In order to describe the charge transport in GNRs endowed with impurities, we present a two-dimensional version of the Su-Schrieffer-Heeger (SSH) Hamiltonian [18], modified to include an external electric field and impurity effects, as follows

$$H = - \sum_{\langle i,j \rangle, s} (t_{i,j} C_{i,s}^\dagger C_{j,s} + h.c.) + \sum_{\langle i,j \rangle} \frac{K}{2} y_{i,j}^2 + \sum_i \frac{p_i^2}{2M} + \zeta_m C_{m,s}^\dagger C_{m,s}, \quad (1)$$

where  $\langle i,j \rangle$  denotes summing over nearest-neighbor sites. Considering the electronic part of our model Hamiltonian,  $C_{i,s}$  denotes the annihilation operator of a  $\pi$ -electron with spin  $s$  in the  $i$ -th site, whereas  $C_{j,s}^\dagger$  describes the creation operator in the  $j$ -th site.  $t_{i,j} = [\exp[-i\gamma\mathbf{A}(t)](t_0 - \alpha y_{i,j})]$  is the hopping integral, where  $t_0$  denotes the hopping of a  $\pi$ -electron between neighboring sites in an undimerized lattice,  $\alpha$  is the electron-phonon coupling constant, and  $y_{i,j}$  refers to the relative displacement coordinate between neighboring sites. The electric field is considered by means of the time-dependent vector potential  $\mathbf{A}$  [19].  $\gamma \equiv ea/(\hbar c)$ , with  $a$  being the lattice parameter,  $e$  the absolute value of the electronic charge, and  $c$  the speed of light. The equation  $\mathbf{E} = -(1/c)\dot{\mathbf{A}}$  denotes the relation between the external electric field and  $\mathbf{A}$ . The lattice backbone, in its turn, is described by  $K$ , which is the harmonic constant that denotes a  $\sigma$  bond;  $M$  the mass of the carbon atom, and the parameter  $y_n$ , which is defined as the change in the bond length.  $p_n$  is the conjugated momentum. The last contribution in Eq. (1) refers to the on-site impurity effects on site  $m$ , where  $\zeta_m$  is the impurity strength.

The lattice backbone dynamics is carried out in a classical approach by means of the Euler-Lagrange equations

$$\frac{d}{dt} \left( \frac{\partial \langle L \rangle}{\partial \dot{u}_n} \right) - \frac{\partial \langle L \rangle}{\partial u_n} = 0. \quad (2)$$

Through of the schematic representation shown in Fig. 1, we can express the force experienced by each site in the lattice by a newtonian equation resulting from Eq. (2) as follows

$$M\ddot{y}_{i,j} = -\frac{2K}{3}[y_{k,i} + y_{l,i} + y_{j,m} + y_{j,n} - 4y_{i,j}] + \frac{2\alpha}{3}e^{i\gamma\mathbf{A}}[(B_{k,i}(t) + B_{l,i}(t) + B_{j,m}(t) + B_{j,n}(t) - 4B_{i,j}(t)) + \text{c.c.}] \quad (3)$$

$B_{i,j}(t) = \sum'_{k,s} \psi_{k,s}^*(i,t) \psi_{k,s}(j,t)$  is the term that couples the electronic to the lattice part in the equations of motion. The primed summation represents a sum over occupied states. This equation is numerically integrated through the discretization of time.

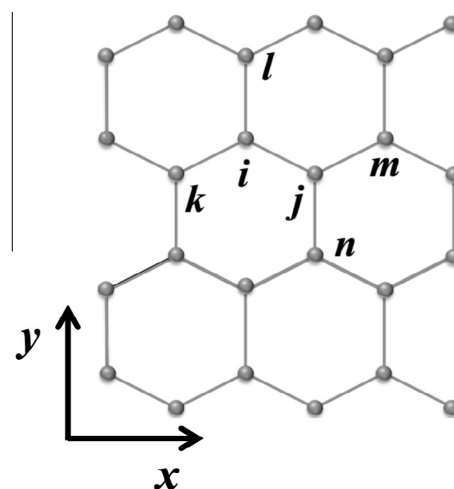


Fig. 1 – Schematic labeling of an armchair GNR.

The electronic part of our model Hamiltonian can be numerically integrated by solving the time-dependent Schrödinger equation (TDSE). The wavefunctions are constructed by means of a linear combination of instantaneous eigenstates. In this way, the solutions of the TDSE are expressed in the form

$$\psi_{k,i}(t + dt) = \sum_l \left[ \sum_m \phi_{l,m}^*(t) \psi_{k,m}(t) \right] e^{(-ie_l dt/\hbar)} \phi_{l,i}(t), \quad (4)$$

where  $\{\phi_{l,i}(n)\}$  and  $\{e_l\}$  are the eigenfunctions and eigenvalues of the Hamiltonian at a given time  $t$  [20]. Here, we have adopted the following values for the parameters:  $t_0 = 2.7$  eV [21–23],  $K = 57$  eV/Å<sup>2</sup> [21], and  $\alpha = 7.6$  eV/Å [24]. According to the literature, these values for  $t_0$  and  $K$  are the most convenient to accurately reproduce the electronic structure features of graphene lattice.  $\alpha$ , the electron-phonon coupling value adopted here, in its turn, is in agreement with the gap energy for armchair GNR experimentally reported [24]. It is worth to stress here that, considering the important problem of non-adiabatic transport, other dynamical methodologies, such as surface hopping methods, should also be considered [25–27].

### 3. Results and discussion

In this work we considered armchair graphene nanoribbons of  $64 \times 6$  size with periodic boundary conditions applied along its length. The width of the GNR is defined by the number of carbon atoms presented in its bottom, i.e., a GNR with dimensions  $64 \times 6$  is composed by 64 atoms along the y-direction and 6 atoms along the x-direction (see Fig. 1). The width is defined as  $6 \times a \times \cos 30^\circ$  whereas the length is defined as  $64 \times a$ , where  $a$  is the lattice parameter. So, the notation  $64 \times 6$  represents an armchair GNR with width  $6 \times 1.40 \times \cos 30^\circ = 7.27$  Å and length  $64 \times 1.40 = 89.6$  Å. The present model simulates a system with single-site impurities which were placed in the sites 132 and 133 of the lattice. Note that, according the convention adopted in our manuscript, the atom index increases from the left to the right in the x-direction and upward in the y-direction, as reported in one of our previous works [23]. It is worthy to stress that such positions were strategically chosen in the lattice in order to promote the collision of the whole polaron with the impurities. This is important because the polaron profile presents charge distribution localized in the two edges of the GNR through its length, with a less charged space in the middle.

Several impurity values and electric field strengths were considered in order to investigate their effects over the polaron dynamics in GNRs. We begin our discussion by investigating the influence of the impurity strength on the charge localization, as depicted in Fig. 2. Two impurities of the same intensity were symmetrically considered in the two sides of the lattice width, around 45 Å, i.e. half, of its total length of 90 Å. This system picture is chosen in order to prevent an asymmetry on the charge interaction. Each stripe stands for a GNR in which the correspondent value of impurity is expressed on the top of the figure. As we simulate a lattice with an electron less than the number of sites as our initial condition, Fig. 2 presents the positive charge distribution

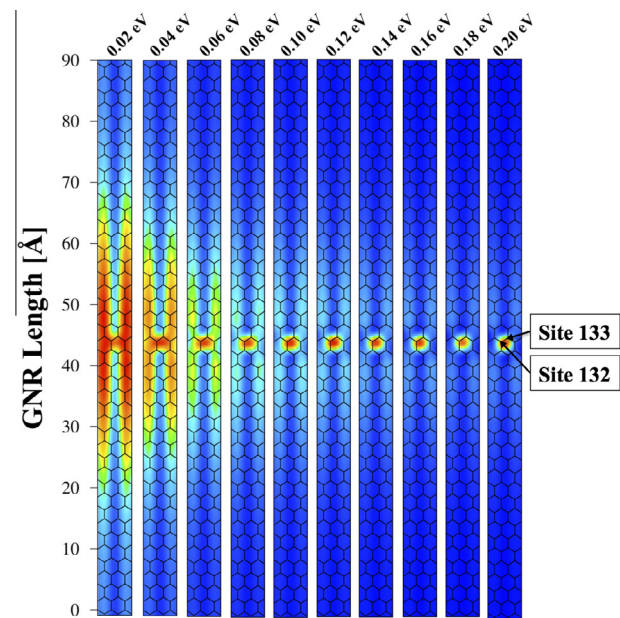


**Fig. 2 – Charge localization as a function of the impurity intensity. The single-site impurities are placed in the sites 132 and 133. (A color version of this figure can be viewed online.)**

shortly after the lattice relaxation, i.e., around 4 fs. For the first stripe, concerning  $\zeta = 0.02$  eV, we can see that half of the net charge tends to be trapped by each impurity. This fact naturally arises from the symmetry of the system. Also, one can see that most of the charge is concentrated above the two centers that corresponds to the impurities. When a stronger impurity,  $\zeta = 0.04$  eV, is considered, two main differences are observed. First, the charge localization is higher, as can be evaluated from the smaller area occupied by the charge in the nanoribbon. Second, although the charge distribution remains symmetrical, one can see that most of the charge is concentrated in between the impurities rather than above each one of them. This pattern of increasing localization with increasing impurity strength is also observed for the other values, as can be seen for the other stripes. From  $\zeta = 0.06$  eV on, we can see a clear decreasing of the area occupied by the charge together with the increase of charge in the region between the two impurities.

The bottom line is that, at least for static simulations, impurities clearly tend to gather the extra amount of charge in the system. The higher is the impurity intensity, the more charge it tends to concentrate around a small region. It should be stressed, though, that this charge concentration does not necessarily mean charge trapping. This point is addressed by the dynamics simulation of Fig. 3, for  $\zeta = 0.02$  eV impurities, subjected to two different electric fields: 0.2 mV/Å (Fig. 3a) and 0.6 mV/Å (Fig. 3b). Fig. 3a, therefore, consists of the time evolution of the first stripe in Fig. 2. Interestingly, the charge concentration caused by the impurity gives rise to a polaron initially in the center of the nanoribbon. The quasiparticle feature of the system is confirmed by the collective behavior the positive charge presents when affected by the electric fields that points down. After the transient time

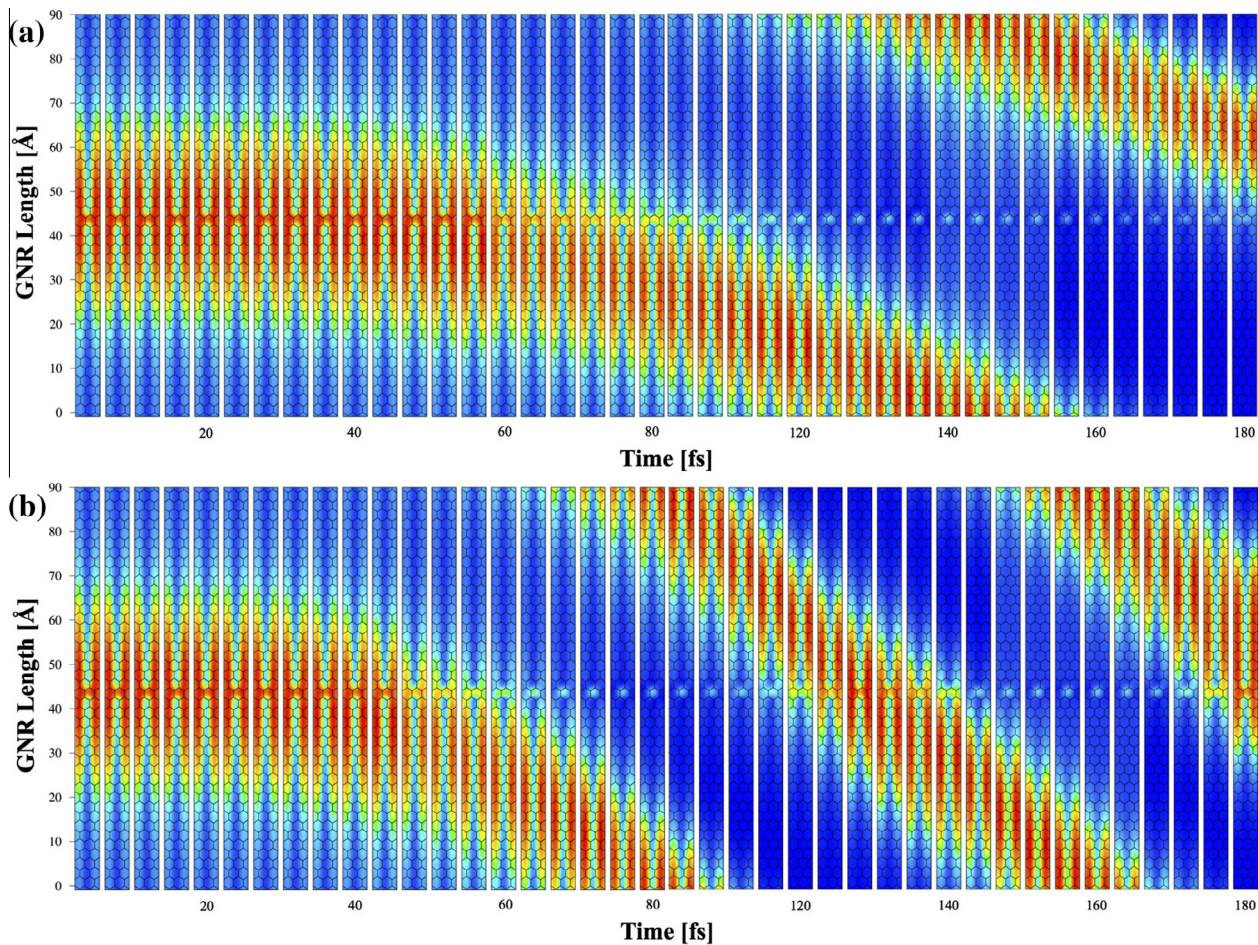


**Fig. 3 – Time evolution of a polaron in a (a) 0.2 and a (b) 0.6 mV/Å electric field. (A color version of this figure can be viewed online.)**

of about 20 fs, the polaron starts to move responding to the electric field. As times goes on, the polaron moves and one can see that its movement is barely affected by the impurity present in the middle of the lattice. After 120 fs, for instance, it is quite clear that the very same impurity that initially broke the system's symmetry, leading concentration of charge that creates the polaron, is now completely decoupled from this quasiparticle. We expect that this low sensibility to the impurity presence by the polaron is due to the low intensity of the former. This point will be further discussed later. Fig. 3b, in its turn, consists in an analogous similar simulation but subjected to a higher electric field. This result confirms the fact that, from the dynamical point of view, the presence of a 0.02 eV impurity is very similar to its absence. Moreover, one can clearly observe the higher velocity of the charge carrier resulting from this higher electric field regime.

In our simulations we adopted the scheme of turning the electric field adiabatically, according reported in reference [28]. This approach is carried out in order to avoid numerical errors that are known to take place when sudden applications are considered. The delay time to the response is due to the fact that, indeed, the electric field is in a transient state, increasing to its final considered value. Furthermore, a straightforward calculation, performed according to reference

[29], shows that the sound velocity in an GNRs is approximately 0.3 Å/fs. For the simulations presented in Fig. 3, the polaron moves with a velocity of about 0.5 Å/fs. The polaron velocity in GNRs is calculated according described in reference [30]. Very recently, we have reported a systematic numerical investigation regarding the polaron dynamics in GNRs (in the absence of impurities) considering several values of electric field strength, GNRs width, and electron-phonon coupling constant [23]. The results reported in this reference contain a phase diagram involving these entities, which may provide a quite embracing physical picture of the polaron transport in GNRs.

Some details regarding the polaron localization in the presence os impurities should now be stressed. The reasons which lead to the polaronic shape presented in Fig. 3 – i.e. extended along the GNR length – were recently discussed in detail in a previous work [22]. On the other hand, the charge localization in the presence of impurities in GNRs (as shown in Fig. 2) is originally reported here. The polaron in organic conductors is a quasi-particle formed due to the strong electron-lattice coupling in these materials. A quasi-particle deforms the lattice through several sites distributing the net charge among them. Therefore, the charge density present in between the single-site impurities is a combined effect of

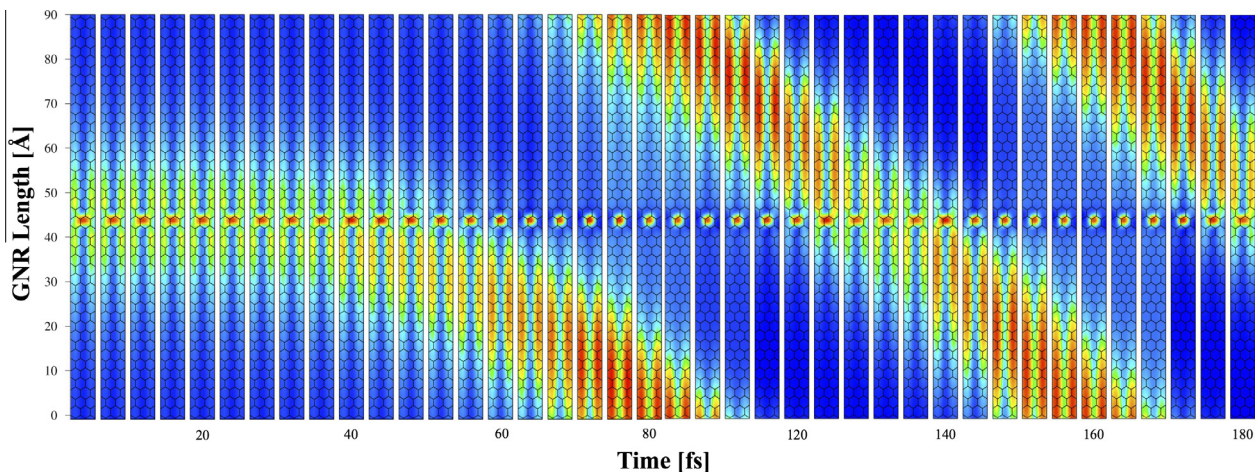


**Fig. 4 – Time evolution of a polaron in a GNR with a 0.06 eV impurity subjected to a 0.6 mV/Å electric field. (A color version of this figure can be viewed online.)**

the charge delocalization of the quasi-particle and the impurity itself.

An interesting way to evaluate whether impurities can play the role of interfering with the movement of the polaron is to perform an investigation considering higher impurity strengths. In Fig. 4 we focus in the simulation with an impurity of 0.06 eV in a GNR subjected to an electric field of 0.6 mV/Å. We can readily note that, in this case, the polaron is no longer unaware of the presence of the impurity. There is a complex balance between the charge held by the impurity and the charge subsequently released by the electric field. Whenever the polaron passes through the impurity region, charge tends to be trapped by the impurity. After that, by dragging the charge together with the polaron, the electric field releases it again to move with the quasi-particle. This interplay between charge periodically concentrated over the impurity and subsequently released by the electric field is an important mechanism that alters the dynamics of a polaron in GNRs. By analyzing impurities of 0.04 eV, we can still observe this phenomena, but in smaller extent.

Virtually no such observations can be made for 0.02 eV. The higher is the impurity strength, the more charge it is capable of holding and, consequently, the more charge the electric field releases. Naturally, this is a mechanism always present.

As we have just seen that high impurities are more likely to cause measurable effects over the polaron dynamics, we now investigate the quasi-particle transport under even higher impurities strengths. Fig. 5 considers the case of a GNR subjected to a 0.6 mV/Å electric field with a 0.1 eV impurity. The first interesting feature to note is that, unlike the previous cases, a considerably smaller charge amount is coupled to the polaron in this case, specially at the beginning of the simulation. One can see that throughout all the simulation the impurity traps most of the net charge given to the system. Again, a similar effect of the electric field taking charge from the impurity by returning to the whole system is observed. Naturally, most of the untrapped charge goes to the quasiparticle defect due to the symmetry breaking it provides. One can see that after around 60 fs, the charge localization associated to the polaron is considerable. Note that,

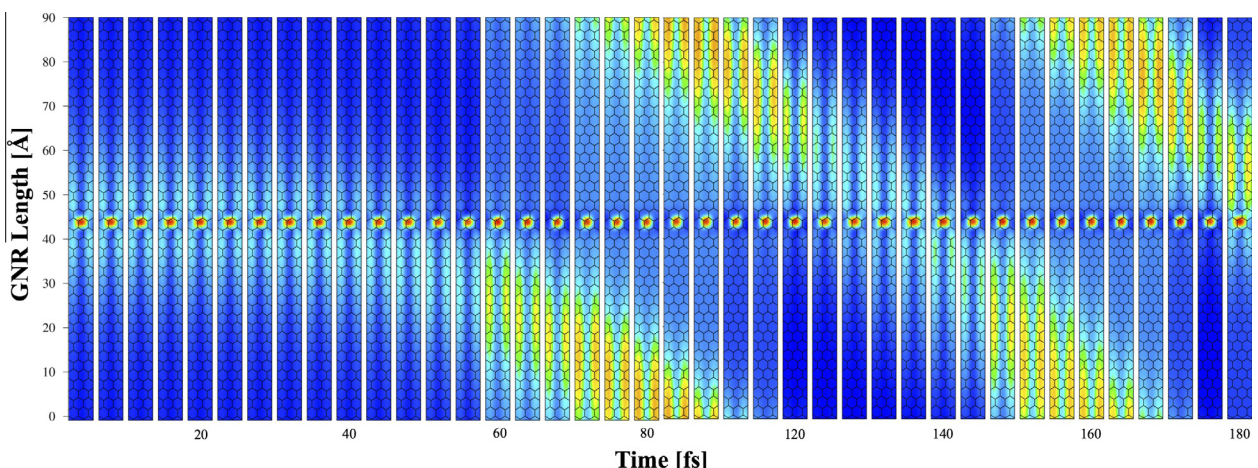


**Fig. 5 – Time evolution of a polaron in a GNR with a 0.1 eV impurity subjected to a 0.6 mV/Å electric field. (A color version of this figure can be viewed online.)**

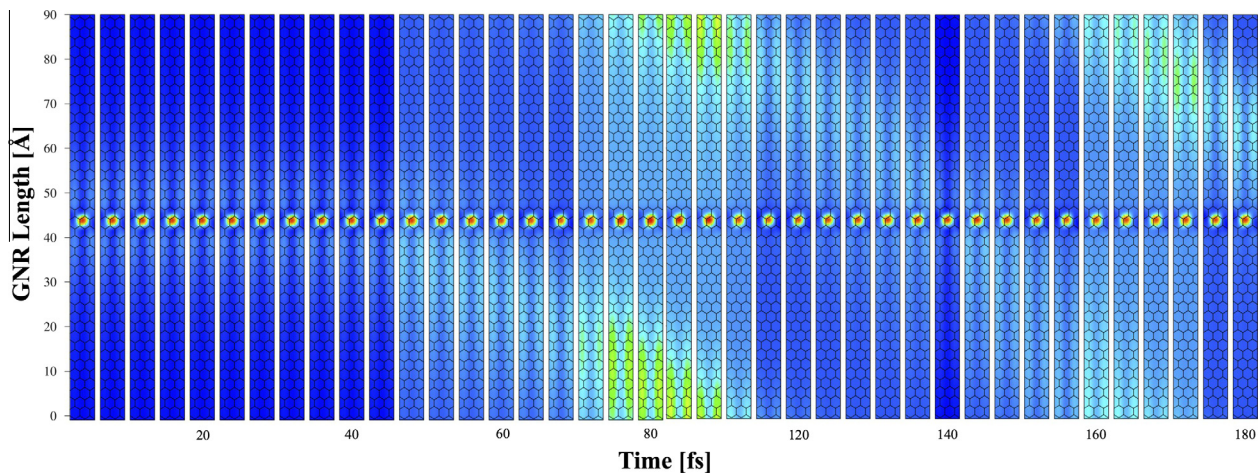


**Fig. 6 – Time evolution of a polaron in a GNR with a 0.2 eV impurity subjected to a 0.6 mV/Å electric field. (A color version of this figure can be viewed online.)**

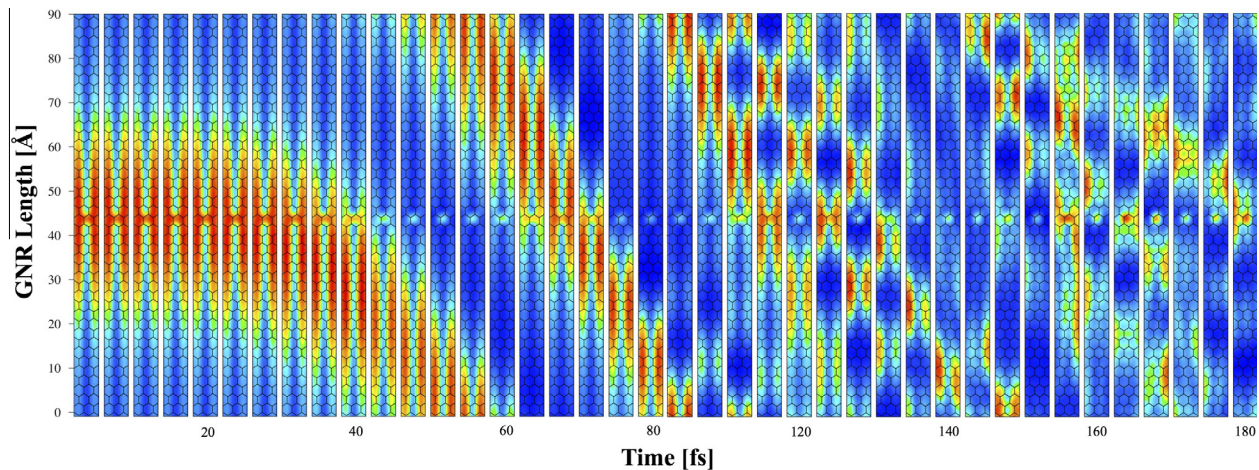


**Fig. 7 – Time evolution of a polaron in a GNR with a 0.2 eV impurity subjected to a 2.0 mV/Å electric field. (A color version of this figure can be viewed online.)**

although the electric field plays the role of untrapping the charge retained by the impurity, through all the simulation the impurity remains considerably charged. Finally, one can see that the polaron movement is strongly affected by the impurity. The trapping mechanism played by the impurity is such that when the polaron passes through the impurity, its own shape is disturbed thus affecting its dynamical properties. Therefore we can now understand how the impurity presence affect the transport properties of GNRs.

A natural question arises concerning whether or not a sufficiently high value of impurity can trap the polaron. In Fig. 6, we repeat the previous simulation doubling the impurity value. We can see that similar results are obtained. At the beginning of the simulation the charge is much more localized over the impurity due to its larger strength. As the time evolves we can observe an increasing localization of the charge over the quasiparticle. Again, whenever the polaron passes through the impurity, it tends to hold charge for a while. This charge is following returned to the polaron under the action of the electric field. The final conclusion is that, for

moderated values of electric field, even high values of impurities are unable to trap the polaron (Fig. 7).

In the last case, we consider the field and impurity effects on the polaron stability. For this we adopt the regime of the high electric field of 2.0 mV/Å accelerating the polaron in a GNR with the small impurity strength of 0.02 eV. As the impurity is small, the charge trap and charge release phenomena played between impurity and electric field is considerably less noticed. Even so, we can note that the impurity has an important effect over the transport mechanism. As we can see, the periodic boundary conditions associated to the high electric field value allows the polaron to pass through the impurity several times. The first time the polaron crosses the impurity that lies in the middle of the chain, it is barely disturbed. However, in this regime the phonon modes created by the high kinetics energy of the polaron are such that the particle eventually loses stability after several collisions. In other words, the faster movement of the polaron due to the higher electric field induces the creation of a higher amount of phonons. The collision between the phonons and the very same

polaron that created them tends to destabilize the quasiparticle. After around 150 fs one can see that the charge is spread over the chain. This fact characterizes the loss of the collective behavior of the polaron. Overall, we obtained that for impurities smaller than 0.1 eV the loss of stability took place for electric fields higher than 0.8 mV/Å. When the impurities were greater than this values the quasiparticle became unstable only for electric fields greater than 1.2 mV/Å.

## REFERENCES

- [1] Stankovich S, Dikin DA, Domke GHB, Kohlhaas KM, Zimney EJ, Stach EA, et al. Graphene-based composite materials. *Nat Lett* 2006;442:282–6.
- [2] Novoselov KS, Geim AK, Morozov SV, Jiang D, Zhang Y, Dubonos SV, et al. Electric field effect in atomically thin carbon films. *Science* 2004;306:666–9.
- [3] Geim AK, Novoselov KS. The rise of graphene. *Nat Mater* 2007;6:183–91.
- [4] Li X, Wang X, Zhang L, Lee S, Dai H. Chemically derived, ultrasmooth graphene nanoribbon semiconductors. *Science* 2008;319:1229–31.
- [5] Yip H-L, Jen AKY. Recent advances in solution-processed interfacial materials for efficient and stable polymer solar cells. *Energy Environ Sci* 2012;5:5994–6011.
- [6] Pumera M. Graphene-based nanomaterials for energy storage. *Energy Environ Sci* 2011;4:668–74.
- [7] Vicarelli L, Vitiello MS, Coquillat D, Lombardo A, Ferrari AC, Knap W, et al. Graphene field-effect transistors as room-temperature terahertz detectors. *Nat Mater* 2012;11:865–71.
- [8] Wehling TO, Yuan S, Lichtenstein AI, Geim AK, Katsnelson MI. Resonant scattering by realistic impurities in graphene. *Phys Rev Lett* 2010;105:056802.
- [9] Pereira VM, Nilsson J, Neto AHC. Coulomb impurity problem in graphene. *Phys Rev Lett* 2007;99:166802.
- [10] Liang S-Z, Sofo JO. Impurity state and variable range hopping conduction in graphene. *Phys Rev Lett* 2012;109:256601.
- [11] Yan J, Fuhrer MS. Correlated charged impurity scattering in graphene. *Phys Rev Lett* 2011;107:206601.
- [12] Bult JB, Crisp R, Perkins CL, Blackburn JL. Role of dopants in long-range charge carrier transport for p-type and n-type graphene transparent conducting thin films. *ACS Nano* 2013;7:7251–61.
- [13] Smith CW, Katoh J, Ishigami M. Impact of charge impurities on transport properties of graphene nanoribbons. *Appl Phys Lett* 2013;102:133502.
- [14] Lherbier A, Blase X, Niquet Y-M, Triozon F, Roche S. Charge transport in chemically doped 2d graphene. *Phys Rev Lett* 2008;101:036808.
- [15] Biel B, Blase X, Triozon F, Roche S. Anomalous doping effects on charge transport in graphene nanoribbons. *Phys Rev Lett* 2009;102:096803.
- [16] Chen L, Wang L, Shuai Z, Beljonne D. Energy level alignment and charge carrier mobility in noncovalently functionalized graphene. *J Phys Chem Lett* 2013;4:2158–65.
- [17] Terrones H, Ruitao L, Terrones M, Dresselhaus MS. The role of defects and doping in 2d graphene sheets and 1d nanoribbons. *Rep Prog Phys* 2012;75:062501.
- [18] Su WP, Schrieffer JR, Heeger AJ. Solitons in polyacetylene. *Phys Rev Lett* 1979;42:1698–701.
- [19] e Silva GM. Electric-field effects on the competition between polarons and bipolarons in conjugated polymers. *Phys Rev B* 2000;61:10777–81.
- [20] Lima MP, e Silva GM. Dynamical evolution of polaron to bipolaron in conjugated polymers. *Phys Rev B* 2006;74:224303.
- [21] Neto AHC, Guinea F, Peres NMR, Novoselov KS, Geim AK. The electronic properties of graphene. *Rev Mod Phys* 2009;81:109–62.
- [22] de Oliveira Neto PH, Teixeira JF, da Cunha WF, Gargano R, e Silva GM. Electron-lattice coupling in armchair graphene nanoribbons. *J Phys Chem Lett* 2012;3:3039–42.
- [23] Junior LAR, da Cunha WF, de Almeida Fonseca AL, e Silva GM, Stafström S. Polaron transport in graphene nanoribbons. *J Chem Phys Lett* 2015;6:510–4.
- [24] Yan J, Zhang Y, Goler S, Kim P, Pinczuk A. Raman scattering and tunable electron-phonon coupling in single layer graphene. *Sol State Commun* 2007;143:39–43.
- [25] Wang L, Prezhdo OV. A simple solution to the trivial crossing problem in surface hopping. *J Phys Chem Lett* 2014;5:713–9.
- [26] Wang L, Beljonne D. Flexible surface hopping approach to model the crossover from hopping to band-like transport in organic crystals. *J Phys Chem Lett* 2013;4:1888–94.
- [27] Wang L, Trivedi D, Prezhdo OV. Global flux surface hopping approach for mixed quantum-classical dynamics. *J Chem Theory Comput* 2014;10:3598–605.
- [28] Ribeiro LA, da Cunha WF, Neto PHO, Gargano R, e Silva GM. Effects of temperature and electric field induced phase transitions on the dynamics of polarons and bipolarons. *New J Chem* 2013;37:2829–36.
- [29] Vos FLJ, Aalberts DP, van Saarloos W. Simple method for calculating the speed of sound in tight-binding models: application to the Su-Schrieffer-Heeger model. *Phys Rev B* 1996;53:R5986–9.
- [30] Ribeiro Junior LA, Stafström S. Polaron stability in molecular semiconductors: theoretical insight into the impact of the temperature, electric field, and system dimensionality. *Phys Chem Chem Phys* 2015;17:8973–82.